CORE
Metadata, citation and similar papers at core.ac.uk
Provided by Nottingham ePrints

Experimental study on a novel photovoltaic thermal system using amorphous silicon cells deposited on stainless steel

Jing Li[a,b], Xiao Ren[a], Weiqi Yuan[a], Zhaomeng Li[a], Gang Pei[a*], Yuehong Su[b], Çağrı Kutlu[b], Jie Ji[a], Saffa Riffat[b]

[a] *Department of Thermal Science and Energy Engineering, University of Science and Technology of China, 96 Jinzhai Road, Hefei, China*

[b] *Department of Architecture and Built Environment, University of Nottingham, University Park, Nottingham NG7 2RD, UK*

[*]Corresponding author. Tel. /Fax: +86 0551 63601652. E-mail: peigang@ustc.edu.cn

Abstract

Amorphous silicon (a-Si) cells are able to perform better as temperature increases due to the effect of thermal annealing. a-Si cells have great potential to solve or ease the problems of high power temperature coefficient, large thermal stress caused by temperature fluctuation and gradient, and thick layer of conventional crystalline silicon cell-related photovoltaic/thermal (PV/T) collectors. In this paper, an innovative a-Si PV/T system is developed. It is the first time that a-Si cells deposited on stainless steel have been used in a practical PV/T system. The system comprises of two PV/T collectors. In each collector, there are 8 pieces of solar cells in series. Long-term outdoor performance has been monitored. Experimental results on the thermal efficiency (η_{th}), electrical efficiency (η_{PV}) and I-V characteristic are presented. The peak instantaneous $\eta_{th,p}$ was about 42.49% with the maximum $\eta_{PV,p}$ of 5.92% on April 2, 2017. The daily average $\eta_{th,a}$ and $\eta_{PV,a}$ were 32.8% and 5.58%. Accordingly, $\eta_{th,p}$, $\eta_{PV,p}$, $\eta_{th,a}$ and $\eta_{PV,a}$ on October 27 were 43.47%, 5.69%, 38.65% and 5.22 %. During more than half a year operation, no technical failure of the system has been observed. The feasibility of the a-Si PV/T is preliminarily demonstrated by the prototype.

Keywords: amorphous silicon cell; photovoltaic/thermal collector; I-V characteristic; thermal efficiency; electricity efficiency

1. Introduction

Photovoltaic/thermal collectors (PV/T) have a higher utilization ratio of solar energy compared to a solo PV module. The mainstream PV/T systems employ crystalline silicon (c-Si) cells for power generation. There are several drawbacks:

First, efficiency decrement of the cells with the increment in the operating temperature is significant. Common c-Si cells have high power temperature coefficients, which are about -0.41 to -0.50%/ ^{o}C at maximum power point (MPP) in standard test conditions (STC). Given an efficiency of 18% at 25 ^{o}C, the absolute efficiency drop can be 5% if the temperature is elevated to 75 ^{o}C. The decline is expected to be steeper at higher working temperature owing to larger magnitude of the coefficient [1]. In case of c-Si cells, the PV/T working at medium-high temperature calls for economic assessment [2], and it might not have advantage over side-by-side PV and solar collector systems. The characteristic of c-Si cells has limited the PV/T application and generally low grade energy can be supplied, in the form of domestic hot water and air [3].

Second, c-Si PV/T may suffer from low electricity efficiency in the seasons when heat is unfavorable. The consumers' demand on heat varies with time and season. Take glazed PV/T-water system in Hefei, China for example. In summer there is remarkable reduction on demand on domestic hot water compared with that in winter, though the solar radiation is more attainable. Water in the storage tank can exceed 70 ^{o}C. Most heat is not desirable and eventually wasted. Meanwhile, it is difficult for the PV/T to function near ambient temperature in regard to the thermal insulation of the system, resulting in a relatively low cell efficiency. This is one of the negative impact of the combined heat and power generation.

Third, c-Si PV/T may be easily broken in the long term operation due to fluctuation in the temperature and its gradient. c-Si cells are commonly laminated on aluminum for the sake of good thermal conductivity. However, coefficient of thermal expansion of c-Si (about 2.6×10^{-6} / ºC at 20 ºC) is far less than aluminum's (about 23×10^{-6} / ºC at 20 ºC) [4]. Since PV/T is likely to experience temperature from 0 to 80 ºC and heat flux from 0 to 600W/m^2 through the year [3, 5], it can be broken by the large mechanical stresses in long time usage. Abruption and deformation have been monitored in some practical PV/T systems [6].

Amorphous silicon (a-Si) cells have attracted less attention than the c-Si cells in the PV/T application. In general, a-Si cells have a low conversion efficiency than c-Si cells at room temperature. The optical gap of a-Si cells is about 1.7eV, which causes photons with the photoelectron energy below 1.7eV to directly pass through the a-Si layer and cannot be absorbed by the intrinsic layer, thus contributing essentially no photocurrent and limiting the conversion efficiency of the a-Si cells. One compelling characteristic of a-Si cells is the degradation in the power output when exposed to the sunlight [7，8], which is known as Staebler-Wronski (S-W) effect [9]. The S-W effect is related with the light-induced degradation of electrical performance and the creation of defect states. After prolonged exposure to sunlight the defect states tend to saturate, and such stability is known as degraded steady state (DSS) [10]. It is not difficult to achieve an initial a-Si cells efficiency of 10%, but it will drop to 7% or lower at stabilized state, depending on the inner structure and operating temperature. The phenomenon has limited the development of a-Si cell despite of its relatively low cost, and makes it less competitive with c-Si cells. a-Si cells are mainly used for sole power generation nowadays. Lower ambient temperature could contribute to more remarkable S-W effect.

However, the aforementioned problems associated with the c-Si PV/T system can be solved or eased by using a-Si cells. a-Si cells benefit from thermal annealing at high operating temperature (>50 ºC) and have the reversible ability to reduce defect states and even can be restored to the original state, leading to an improved power generation. In contrast to c-Si cells, a-Si cells may have positive power temperature coefficients. It has been demonstrated that the S-W effect can be weakened in the high temperature stage [11]. According to the annual performance of a-Si PV modules, the electrical efficiency of a-Si PV modules has seasonal variation which is different from c-Si PV modules [12-14]. a-Si PV modules have a higher electrical efficiency in summer months and lower electrical efficiency in winter months, and the opposite is true for c-Si PV modules. The seasonal variation of a-Si PV modules is attributed to the S-W effect and spectral effect [13]. The degradation at low temperature (22±8 ^{o}C) for about 1000h could be recovered upon the subsequent warm soaking (51±8 ^{o}C) for about 500h, resulting in an efficiency increment between 10% and 17% [15]. The operating temperature during light-soaking has been deemed as the most important factor for determining stabilized cell performance [16]. Based on tests on the PV systems over four years, it was concluded that the a-Si cells exhibited positive power temperature coefficient. In some cases the power of a-Si was increased by as much as 8.4% due to thermal annealing [17]. For a different climate or cell configuration (e.g. i-layer thicknesses), the best a-Si cell at STC may not have the best annual energy yield [18]. a-Si PV modules can operate up to 100 ^{o}C with only small amount of power losses [19]. Higher temperature could result in faster stabilization and higher efficiency at DSS [20].

The power temperature coefficient of a-Si cells at DSS may be positive, which is inconsistent with results in the international standard test condition. The reason is duration of measurement defined in such standard is typically short, and the cell is unable to proceed with a full annealing as the operation temperature rises. Evidences have shown the power temperature coefficient of a-Si cells for a short time scale of several hours is negative, while it is positive for a longer time scale of seasons. In fact, a-Si modules continue to show further change in maximum power even after they stabilize according to the international qualification standard IEC 61646 [21]. It indicates that the high operating temperature improves the electrical performance of a-Si PV modules as a result of thermal annealing.

Aside from the unique positive power temperature coefficient in long term operation, the thin-film a-Si cells can be easily deposited at low temperature onto a variety of substrates such as glass, stainless steel sheet and plastic sheet [22] and there are savings on silicon material. When deposited on stainless steel, the a-Si cells are flexible. The panels are used commercially and can be rolled up and carried in a backpack and used to charge the electrical devices like laptops. They may be able to cope with interruption at fluctuating temperature. Owing to the thin-film, the cells should have lower thermal resistance than mainstream c-Si cells.

The above characteristics of a-Si cells are desirable in the PV/T application. a-Si PV/T collectors shall normally work at higher temperature than ambient temperature, which will facilitate better thermal annealing, and thus the electrical performance can be improved. The cells may benefit from high temperature operation even in seasons of less demand on heat and would not have a dramatic efficiency drop as c-Si cells. The modules possess good thermal conductivity and can avoid huge thermal stress.

Above all, a-Si PV/T system is promising. Theoretical works have been reported. The performances of a-Si and c-Si PV/T have been compared and analyzed by simulation [23]. The effect of high-temperature annealing strategy on the annual yield of a-Si PV/T has been examined. Significant amount of additional energy generation is possible over the year with an appropriate dispatch strategy at thermal annealing temperature of 100 ^{o}C [20, 24]. The thickness of a-Si intrinsic layer has also influence on the a-Si PV/T performance [25]. Upon annealing, the grown-in SiH monohydride groups are partially transformed into SiH2 dihydrides and polysilane chains which have been reported to impair the performance of a-Si:H based PV/T devices [26]. Compared with c-Si cells, a-Si cells are more suitable for operating at the medium-high temperature, and are promising in solar roof [27-29], PV glazing [30] and photovoltaic-thermoelectric [31-34] applications.

So far, there have been a few reports on the experimental study of a-Si PV systems such as a-Si PV windows which can provide daylight illuminance and electricity generation simultaneously [35-36] and a-Si PV walls [37]. The field tests of systems for residential application have been done in Bangkok, Thailand, with an average electricity efficiency of 4.0% and thermal efficiency of 51% [38]. Investigation on a heat pipe a-Si PV/T system has been done in Changsha, China, with an average electricity efficiency of 4.8% and thermal efficiency of 41% [39]. In these studies, the substrate for the a-Si cells is glass or plastic.

Notably, experimental investigation on a-Si PV/T system using stainless steel as the substrate has not been reported yet. Its thermodynamic performance and technical practicability need to be demonstrated. In this paper, design and test of a novel PV/T system using a-Si cells is introduced. To the best of the authors' knowledge, it is the first time that a-Si cells deposited on stainless steel have been used in a practical PV/T system. Outdoor performance and simulation of the system is investigated. The thermal efficiency, electrical efficiency and the I-V characteristic are analyzed in detail. Feasibility of the system is discussed on the basis of over half a year running.

Nomenclature		λ	thermal conduction, W/(m·K)
A	area, m^2	ρ	density, kg/m^3, reflectance, -
B	temperature coefficient, K^{-1}	σ	Stefan-Boltzman constant, $W/(m^2 \cdot K^4)$
c	specific heat capacity, J/(kg·K)	τ	transmittance, -
D	diameter, m	$(\tau\alpha)$	effective absorptance, -
d	thickness, m, inner diameter, m	ξ	covering factor, -
E	electrical gain, W	*Subscripts*	
G	solar irradiation, W/m^2	a	ambient, air
h	heat transfer coefficient, $W/(m^2 \cdot K)$	ad	adhesive layer
L	length, m	b	absorber plater
$\dot{m}$	mass flow rate, kg/s	bt	welding layer
$\dot{M}$	total mass flow rate, kg/s	e	sky
M	mass, kg	g	glass
R	thermal resistance	i	insulation layer
T	temperature, K	in	inlet of collector
t	time, s	out	outlet of collector
u	flow velocity, m/s	PV	PV module
Nu	Nusselt number, -	ref	standard test condition
Ra	Raleigh number, -	t	copper tube

P	Perimeter, m	tank	water-storage tank
Greek letters		TPT	black TPT
α	absorptivity, -	w	water
β	tilt angle of collector, ^{o}	wt	water in the tank
ε	emissivity, -		
η	efficiency, -		

2. Description of the a-Si PV/T collector

Triple-junction a-Si cells are employed (a-Si:H/a-SiGe:H/a-SiGe:H), provided by Xunlight Kunshan Co.,Ltd. The schematic structure is depicted in Fig.1. The peak quantum efficiencies of a-Si top-cell, a-SiGe middle-cell, a-SiGe bottom-cell are about 67% at 450nm, 55% at 580 nm and 48% at 710 nm, with a total QE efficiency of up to 86% [40].

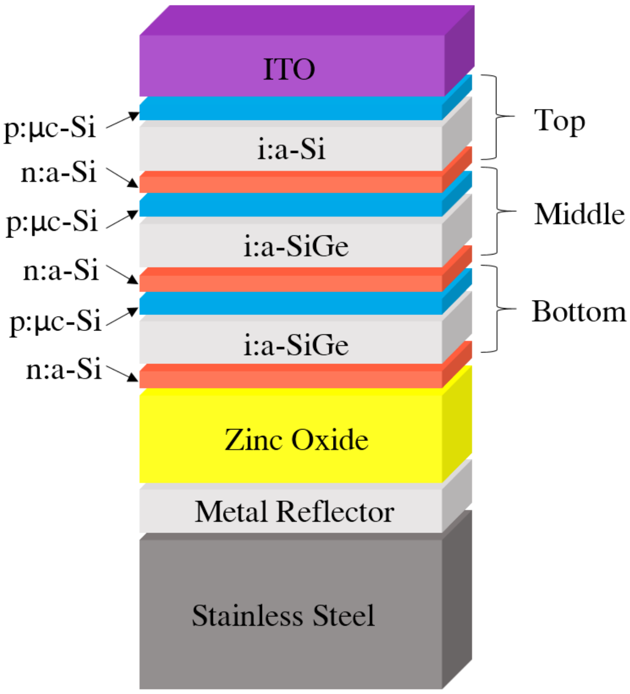

Fig.1. Schematic diagram of the triple-junction a-Si cells

The cross section and the structure diagram of the novel PV/T module are depicted in Figs. 2 and 3. The a-Si PV/T collector has the following components: glass cover, a-Si cells, aluminum absorber plate, copper tubes and thermal insulation layer. The glass cover utilizes a textured inner face. To encapsulate the a-Si cells, transparent tedlar-polyester-tedlar (TPT), black TPT and EVA are employed. The transparent TPT can make solar irradiation through and protect the a-Si cells, and it can make the a-Si cells electrical insulated. The EVA plays a role in preventing water and dirt, as well as in tight bonding with other parts. The encapsulation of the a-Si PV/T is similar with that of c-Si ones.

The thickness of the glass cover, transparent TPT, EVA, PV cell, black TPT, aluminum absorber plate is about 3.2, 0.2, 0.2, 0.6, 0.2 and 1.16 mm, respectively. There is a 26 mm air gap between the glass cover and the PV module to reduce the convective heat transfer. The bottom of the a-Si PV/T collector is a thermal insulation layer of 36 mm in order to reduce the conductive heat loss.

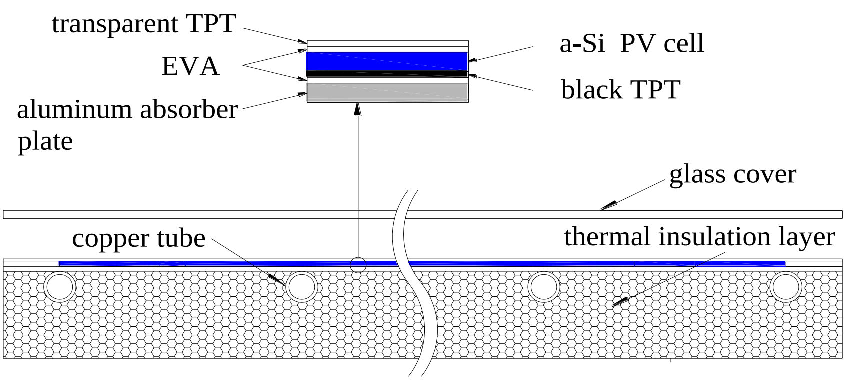

Fig. 2. Cross section of a-Si PV/T collector

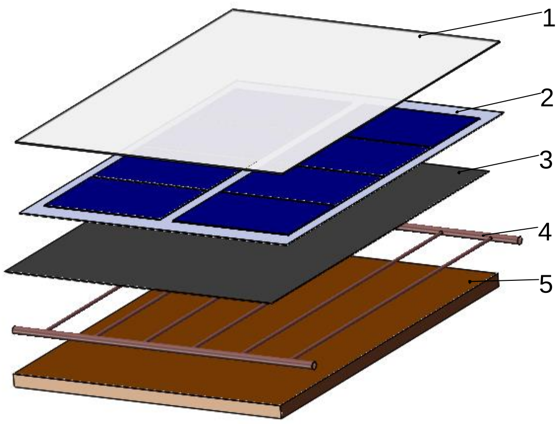

Fig. 3. Structure diagram of the a-Si PV/T collector: 1-glass cover; 2-amorphous silicon cells; 3-aluminum absorber plate; 4-copper tubes; 5-thermal insulation layer

An unpacked a-Si cell is shown in the Fig. 4. The flexible cell has stainless steel as the substrate. Eight pieces of a-Si cells in series are laminated onto the surface of the aluminum absorber plate. The size of one piece of a-Si cell is 356 mm × 239 mm. The photovoltaic characteristics of an a-Si cell are listed in Table 1 in the standard test conditions (irradiation of 1000W/m^2 and temperature of 25 ^{o}C). The data are related to the cell performance prior to degradation.

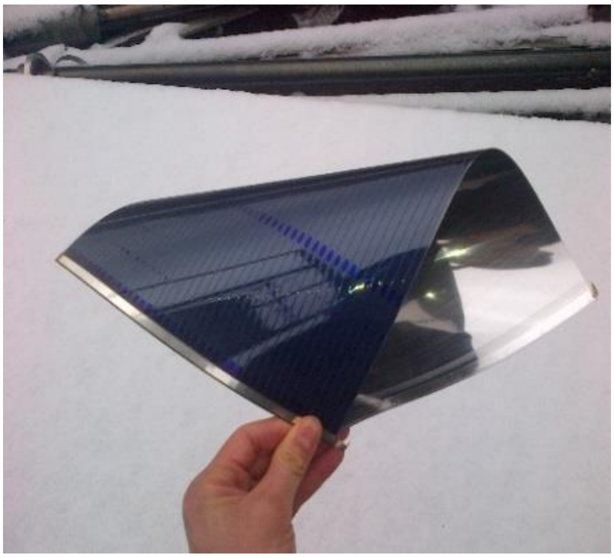

Fig. 4. An unpacked a-Si cell

Table 1 Photovoltaic characteristics of an amorphous silicon cell in standard test condition

Parameter	Value
Power (±10%)	P_m=6.5W
Open circuit voltage	V_{oc} =2.1V
Short circuit current	I_{sc}=5.1A
Voltage at max power	V_m=1.6V
Current at max power	I_m=4.1A

The outer dimension of the PV/T collector is displayed in Fig.5. The cells are laminated on the aluminum absorber plate of 820 mm × 1100 mm. Six copper tubes are stuck on the back of the plate by laser welding. The dimension of a copper tube is φ10 × 1040 mm and the distance between two adjacent tubes is 150 mm.

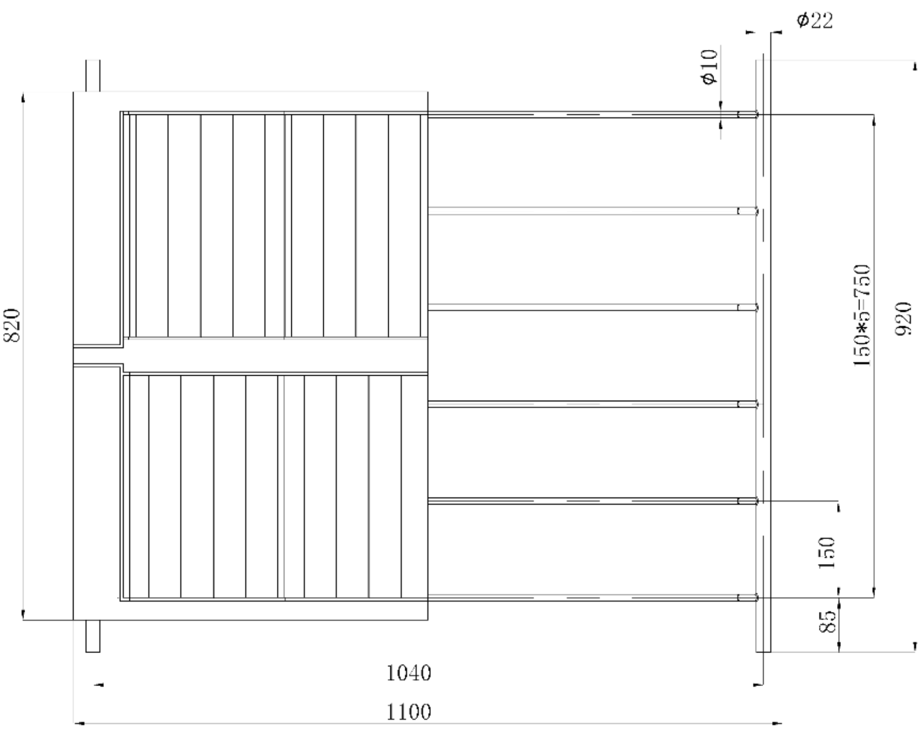

Fig. 5. Outer dimensions of the PV/T

3. Experimental setup

To estimate the performance of the a-Si PV/T collectors, the experimental system has been established on the roof of a building in Hefei which is located at 117.27E longitude and 31.86 N latitude. The test rig and schematic diagram of the a-Si PV/T system are presented in Figs. 6 and 7. The cooling water of the PV/T system circulates in a closed loop. Two a-Si PV/T collectors in series, a water-storage tank with the capacity of 80 L, a water pump, pipes, a water flowmeter and a maximum power point tracking (MPPT) PV controller (SSCM-1224-5A) are used in the experiment. The two a-Si PV/T collectors faced the south with a tilt angle of 30° for better utilization of solar irradiation [41]. Details on the measuring instruments are given in the Table 2. The installation angle of the radiometer was the same as that of the collectors to measure the global solar radiation (direct radiation and diffuse radiation) received on the surface of the collectors. The measurement data are recorded and stored on a disk via Agilent Bench Link Date Logger, a computer data-acquisition system.

Fig. 6. Test rig of the a-Si PV/T system

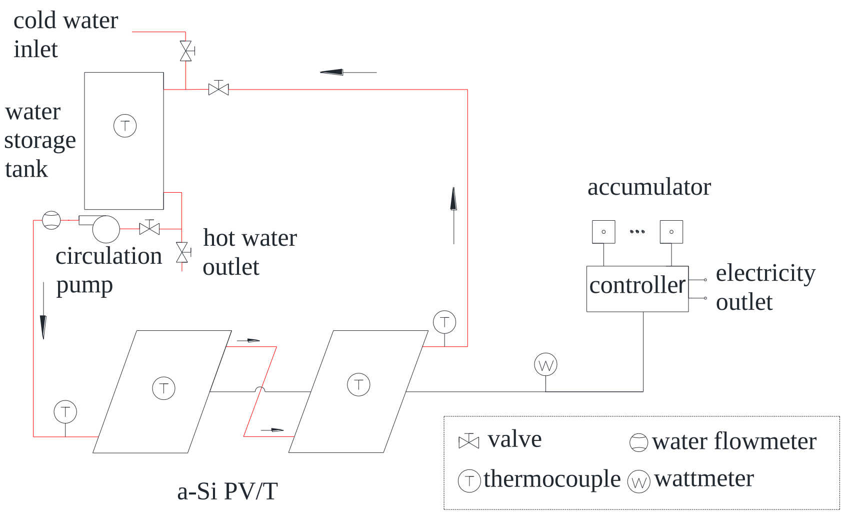

Fig. 7. Schematic diagram of the a-Si PV/T system experimental setup

Table 2 Types of related measuring instruments

Instruments	Types	Measurement accuracy	Location
Thermal resistance	Pt 100	±0.1 °C	Collector inlet and outlet
Thermocouple	Type T	±0.5 °C	Water-storage tank; ambient ; aluminum absorber
Flowmeter	LWGY	±5%	Water-storage tank output
Radiometer	TBQ-2	±2%	Solar collector
Current sensor	HKK-13-I	±0.1%	PV module output current

4. Mathematic models

4.1 Mathematic models of the a-Si PVT system

Simulation is carried out to provide a closer view of the heat transfer and power generation in the system. The following assumptions are made [6]:

1) The water flow rate in the copper tube is uniform.

2) The heat capacities of the adhesive layers (EVA and TPT) are neglected.

3) The temperature gradients of the glass cover, PV module, absorber plate and copper pipe in thickness are negligible.

The energy balance equation of glass cover can be expressed as:

$$\rho_g c_g d_g \frac{\partial T_g}{\partial t} = h_a(T_a - T_g) + h_{e,g}(T_e - T_g) + h_{g,PV}(T_{PV} - T_g) + G\alpha_g \tag{1}$$

Where h_a, $h_{e,g}$, $h_{g,PV}$ are the convective heat transfer coefficient between the glass cover and the surrounding air, the radiant heat transfer coefficient between the glass cover and the sky, and the heat transfer coefficient between the glass cover and the PV module, respectively, expressed as:

$$h_a = 2.8 + 3.0u_a \tag{2}$$

$$h_{e,g} = \varepsilon_g \sigma (T_e^2 + T_g^2)(T_e + T_g) \tag{3}$$

$$h_{g,PV} = \sigma(T_{PV}^2 + T_g^2)(T_{PV} + T_g)\left(\frac{\xi}{1/\varepsilon_{PV} + \xi(1/\varepsilon_g - 1)} + \frac{1-\xi}{1/\varepsilon_{PV} + (1-\xi)(1/\varepsilon_g - 1)}\right) + \frac{Nu \cdot \lambda_a}{d_a} \tag{4}$$

Where ξ is covering factor defined as:

$$\xi = \frac{A_{PV}}{A_b} \tag{5}$$

For inclination angle of the collector ranging from 0° to 75°, the Nusselt number can be calculated as [42]:

$$Nu = 1 + 1.14\left(1 - \frac{1708(\sin 1.8\beta)^{1.6}}{Ra \cdot \cos\beta}\right)\left[1 - \frac{1708}{Ra \cdot \cos\beta}\right]^+ + \left[\left(\frac{Ra \cdot \cos\beta}{5830}\right)^{1/3} - 1\right]^+ \tag{6}$$

Where $[]^+$ indicates that only positive values for terms within square brackets shall be used;

in the case of negative values, zero is used.

The two-dimension energy balance equation for PV module is expressed as:

$$\xi\rho_{PV}c_{PV}d_{PV}\frac{\partial T_{PV}}{\partial t}=\lambda_{PV}d_{PV}\left(\frac{\partial^2 T_{PV}}{\partial x^2}+\frac{\partial^2 T_{PV}}{\partial y^2}\right)+h_{g,PV}\left(T_g-T_{PV}\right)+\left(T_b-T_{PV}\right)/R_{b,PV} \\ +G\left(\tau\alpha\right)_{PV}-\xi E_{PV} \tag{7}$$

Where $(\tau\alpha)_{PV}$ and E_{PV} are the effective absorptance and the output power of the PV cells (W/m^2), respectively, and expressed as:

$$\left(\tau\alpha\right)_{PV}=\frac{\tau_g\tau_{ad}\alpha}{1-\left(1-\alpha\right)\rho_d} \tag{8}$$

$$E_{PV}=G\tau_g\tau_{ad}\eta_{ref}\left[1-B\left(T_{PV}-T_{ref}\right)\right] \tag{9}$$

Where ρ_d is the reflection of glass cover for diffuse radiation; α is the comprehensive absorptance, expressed as:

$$\alpha=\xi\alpha_{PV}+\left(1-\xi\right)\alpha_{TPT} \tag{10}$$

The $R_{b,PV}$ is the thermal resistance of the adhesive layer between the PV module and the absorber plate ($m^2\cdot K/W$) and expressed as:

$$R_{b,PV}=\frac{d_{ad}}{\lambda_{ad}} \tag{11}$$

For the absorber plate, some nodes are in connection with the copper tubes and heat is transferred directly from the nodes to the tubes. Meanwhile, some nodes are set between the tubes. There are two types of energy balance equations, which are related to the connection nodes and middle nodes, respectively.

The energy balance equation of the middle nodes is expressed as:

$$\rho_b c_b d_b\frac{\partial T_b}{\partial t}=\lambda_b d_b\left(\frac{\partial^2 T_b}{\partial x^2}+\frac{\partial^2 T_b}{\partial y^2}\right)+\left(T_{pv}-T_b\right)/R_{b,PV}+\left(T_a-T_b\right)/R_{b,a} \tag{12}$$

The energy balance equation of the connection nodes is expressed as:

$$\rho_b c_b d_b \frac{\partial T_b}{\partial t} = \lambda_b d_b \left(\frac{\partial^2 T_b}{\partial x^2} + \frac{\partial^2 T_b}{\partial y^2} \right) + \left(T_{pv} - T_b \right) / R_{b,PV} + \frac{T_t - T_b}{R_{b,t} \cdot A_{ij}} \tag{13}$$

Where A_{ij} is the area of a single controller (m^2), $R_{b,a}$ and $R_{b,t}$ are the thermal resistance between the absorber plate and the air (m^2·K/W), and the thermal resistance between the absorber plate and the copper pipe (K/W), expressed as:

$$R_{b,a} = d_i / \lambda_i + 1/h_a \tag{14}$$

$$R_{b,t} = d_{bt} / \left(\lambda_{bt} \cdot A_{bt} \right) \tag{15}$$

The energy balance equation of the copper tube is expressed as:

$$\pi \frac{\left(D_t + d_t\right)}{2} \frac{\left(D_t - d_t\right)}{2} \rho_t c_t \frac{\partial T_t}{\partial t} = \pi \frac{\left(D_t + d_t\right)}{2} d_t \lambda_t \frac{\partial^2 T_t}{\partial x^2} + \pi d_t h_{w,t} (T_w - T_t) + \frac{T_b - T_t}{R_{b,t} \cdot dx} \tag{16}$$

Where $h_{w,t}$ is the convective heat transfer coefficient between the copper tube and flowing water.

For the flowing water in the copper tube, the energy balance equation is expressed as:

$$A_t \rho_w c_w \frac{\partial T_w}{\partial t} = -\dot{m} c_w \frac{\partial T_w}{\partial x} + A_t \lambda_w \frac{\partial^2 T_w}{\partial x^2} + P_t h_{w,t} \left(T_t - T_w \right) \tag{17}$$

The energy balance equation of water in the tank is expressed as:

$$A_{tank} \rho_w c_w \frac{\partial T_{wt}}{\partial t} = -\dot{M} c_w \frac{\partial T_{wt}}{\partial x} + A_{tank} \lambda_w \frac{\partial^2 T_{wt}}{\partial x^2} + P_{tank} h_{tank} \left(T_a - T_{wt} \right) \tag{18}$$

Where h_{tank} is the heat transfer coefficient between the surrounding air and water in the tank.

4.2 Performance evaluation

The thermal and electrical efficiencies are two important parameters in evaluating the system performance. The instantaneous thermal efficiency of the a-Si PV/T collectors is defined as ratio of the heat gain to the incident solar radiation.

$$\eta_{th} = \frac{Q_w}{G A_b} = \frac{c_w \dot{M} (T_{out} - T_{in})}{G A_b} \tag{19}$$

The fitted curve of the instantaneous thermal efficiency under quasi-steady-state conditions is displayed. A linear correlation between the instantaneous thermal efficiency and the reduced temperature $(T_{in} - T_a)/G$ is built, expressed as [43]:

$$\eta_{th} = F_R(\tau\alpha)_e - F_R U_L \frac{T_{in} - T_a}{G} \quad (20)$$

Where $F_R(\tau\alpha)_e$ is the intercept efficiency when the inlet temperature is equal to the ambient temperature, $F_R U_L$ is the coefficient of heat loss.

The instantaneous electrical efficiency is represented by:

$$\eta_{PV} = \frac{E_{PV}}{GA_{PV}} = \frac{U_{mp} I_{mp}}{GA_{PV}} \quad (21)$$

A flowmeter is present in the system to measure the water flow rate and a considerable pressure drop exists, thereby leading to more pump power. In the PV/T performance analysis, the pump power is generally not taken into account [3, 5].

For a PV/T system using water as a circulation working fluid and storing solar energy in the tank, the daily average thermal and electrical efficiency can be given by:

$$\eta_{th,a} = \frac{c_w M (\overline{T_{w,f}} - \overline{T_{w,i}})}{HA_b} \quad (22)$$

$$\eta_{PV,a} = \frac{\sum E_{pv} \Delta t}{HA_{PV}} = \frac{\sum U_{mp} I_{mp} \Delta t}{HA_{PV}} \quad (23)$$

Where Δt is the time interval of data acquisition (s), $\overline{T_{w,\iota}}$ and $\overline{T_{w,f}}$ are the initial and final average water temperature in water-storage tank (°C).

Since electricity is a higher grade energy compared to thermal energy, the daily efficiency of the a-Si PV/T system is calculated by the following equation [44]:

$$\eta_{PVT,a} = \eta_{th,a} + \zeta \frac{\eta_{PV,a}}{\eta_{power}} \quad (24)$$

Where $\eta_{PVT,a}$ is the daily comprehensive efficiency of the a-Si PV/T system, η_{power} is the electrical efficiency from the conventional heat-engine plant and its value is 38%.

The fill factor (FF) is defined as the ratio of the product of the current and voltage at the maximum power point to the product of the short circuit current and the open circuit voltage. The FF is an important parameter that affects the output performance of the cells. When the open circuit voltage and short circuit current are constant, the electrical efficiency of the cells depends on the FF. The FF is expressed as:

$$FF = \frac{I_{mp}U_{mp}}{I_{sc}U_{oc}} \tag{25}$$

To evaluation the degree of agreement between the simulation and the experiment, the relative error (RE) is calculated by:

$$RE = \frac{X_{\exp} - X_{sim}}{X_{\exp}} \times 100\% \tag{26}$$

Where the X_{exp} and X_{sim} is the values of experiment and the simulation, respectively.

5. Results and discussion

The construction of the a-Si PV/T system comprised of prolonged work. It started in April 2015. Few lessons could be learned from experiences. Manufacturers of a-Si cells deposited on metal are rare. One module of length of 2.0 m and width of 1.0 m, which was the similar size with conventional solar collectors, had been fabricated previously. However, it failed to function properly, mainly due to the electrode damage in the laminating process. The a-Si cells were much thinner than c-Si cells and the technical requirements on lamination seemed to be higher in order to guarantee uniform pressure and good electric insulation.

To facilitate easier fabrication, the size of the modules was reduced (about 1m×1m). This paper is focused on the recent PV/T modules that were developed in October 2016. It took a few months further to build and commission the whole test rig with proper sensor, battery storage, water tank. During the installation and commission, the modules were carefully covered to avoid exposure to solar radiation. In March 2017, the system was ready for long term operation.

In the following sections, the test results for two sunny days (April 2, 2017 and October 27, 2017) are summarized, which represent the system performance at early-stage degradation and after prolonged exposure, respectively. The variations of a-Si cells' operating temperature, maximum power point current and voltage, inlet and outlet temperature of collectors, water-storage tank temperature together with solar irradiation, water mass flow rate, ambient temperature are displayed. The thermal efficiency, electrical efficiency and the I-V characteristic are examined.

5.1 Test on April 2, 2017

A full day test of the a-Si PV/T system was commenced at 8:30 and concluded at 15:30. The mass flow rate of the two collectors in series was around 0.058 kg/s. Fig. 8 shows the variation of solar irradiation and ambient temperature during the day. Both direction and diffusion are taken into account. The solar irradiation gradually increased in the morning and decreased in the afternoon. At the beginning and end of the test, it was about 474.6 W/m^2 and 426.9 W/m^2, respectively. The maximum value was 989.2 W/m^2 at 11:18. The daily total solar irradiation was 20.33 MJ/m^2. The ambient temperature fluctuated from 13.7 °C to 20.5 °C and the average value was about 19.4 °C.

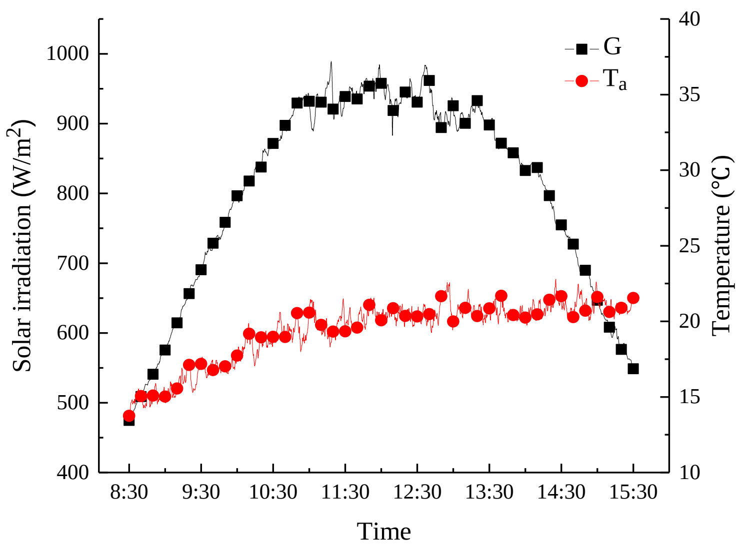

Fig. 8. Variations of solar irradiation and ambient temperature on April 2

The simulation and experiment results of the temperature of aluminum plate and the water in the water-storage, and the temperature of the inlet and outlet during the day are shown in the Fig. 9 and Fig. 10. Simulation results are in good agreement with the test data. Two thermocouples were placed on the middle of the aluminum plate back and the center of the water-storage tank. The test temperature of the water-storage tank increased from 20.2 ^{o}C to 56.0 ^{o}C which can fulfill the domestic demand on hot water. The final temperature of the water in the tank in the simulation is 56.5 ^{o}C. The tested temperature of aluminum plate gradually increased from 25.0 ^{o}C to 62.0 ^{o}C and the simulated values climbed from 25.6 ^{o}C to 61.0 ^{o}C.

According to the test results, the inlet and outlet temperature of the PV/T system had a same trend with the temperature of water-storage tank. The outlet and inlet temperature difference increased in the beginning from 1.1 ^{o}C to 2.9 ^{o}C and then decreased to 0.6 ^{o}C in the afternoon. The tank and water inlet temperatures were very close, indicating that the temperature gradient in the tank was small. On the other hand, there was a difference of about 2-8 ^{o}C between aluminum plate temperature and water inlet/outlet temperature, which was due to the thermal resistance between the plate and water. The difference reached the maximum at the noontime when the heat flux was largest. The daily total heat gain of water-storage tank was 12.03MJ.

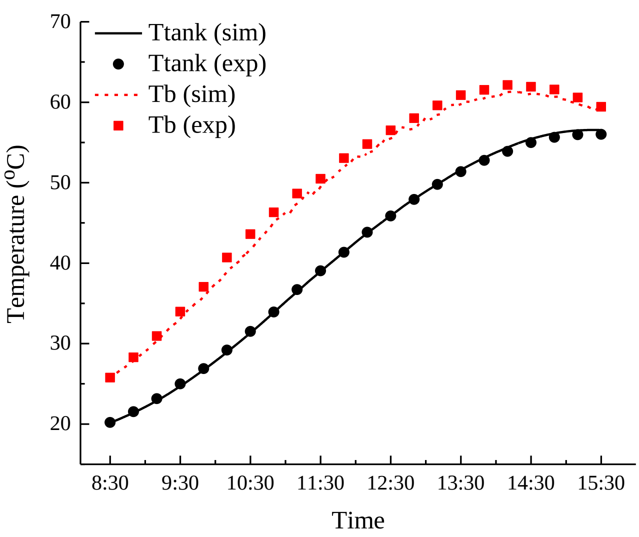

Fig. 9. Simulation and experiment results of the temperatures of the aluminum plate and water in the tank on April 2

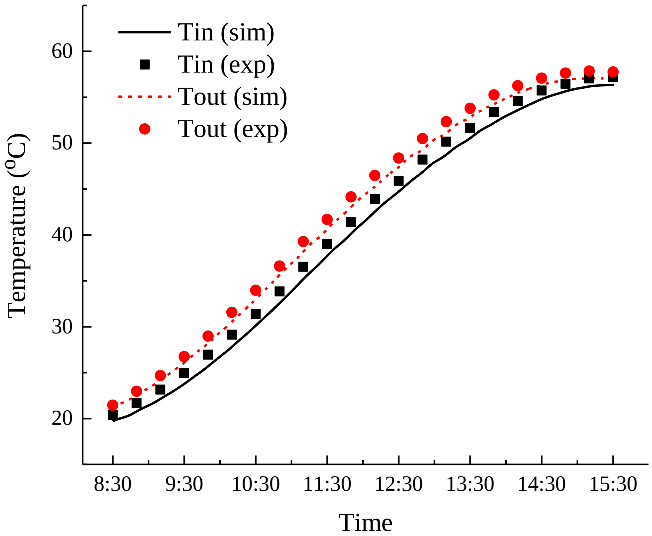

Fig. 10. Simulation and experiment results of water temperatures at the inlet and outlet of the PV/T system on April 2

Fig. 11 displays the variation of heat gain and thermal efficiency with time. The maximum heat gain was 693.61W, corresponding to the maximum thermal efficiency of 42.49% at 11:02. Unlike the solar irradiation which was approximately symmetrical, the thermal efficiency had a drop in the afternoon that was steeper than the increment in the morning. This was attributed to the weaker solar radiation and higher water temperature in the water-storage tank. The daily average thermal efficiency of the a-Si PV/T system was 32.8%. The thermal efficiency was not high in comparison with conventional flat plate collector and there are some reasons: First, the size of a-Si PV/T is relatively small, resulting in more significant heat loss. Second, there is no selective absorption coating on the surface of a-Si cells and the cell has a higher long-wave emissivity and radiative heat loss. Third, since two collectors are connected in series, the connection between the two collectors leads to certain heat loss.

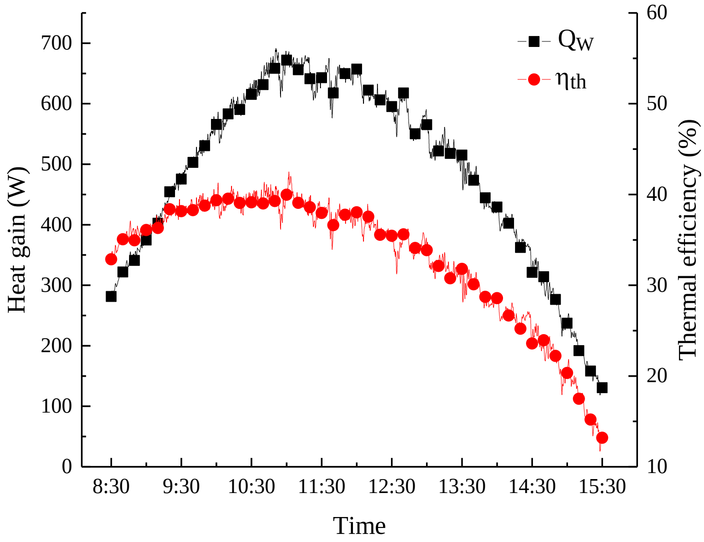

Fig. 11. Variations of heat gain and thermal efficiency on April 2

During the experiment, the system could be considered to operate on quasi-steady conditions in regard to the slow rise in the temperature of water-storage tank. Therefore the thermal efficiency of a-Si PV/T collectors was obtained by the inlet and outlet temperature difference as shown in Fig. 12. The thermal efficiency can be expressed by the regression formula:

$$\eta_{th} = 0.4823 - 5.096\frac{T_{in} - T_a}{G} \tag{27}$$

It is a function of $(T_{in} - T_a)/G$. According to the regression line, the intercept thermal efficiency is 48.23% when the inlet temperature was equal to the ambient temperature, and the coefficient of heat loss is 5.096 W/(m^2·°C). The electrical efficiency of the a-Si PV/T collectors is around 5.58%. Thus the overall intercept efficiency i.e., optical efficiency is 59.3%.

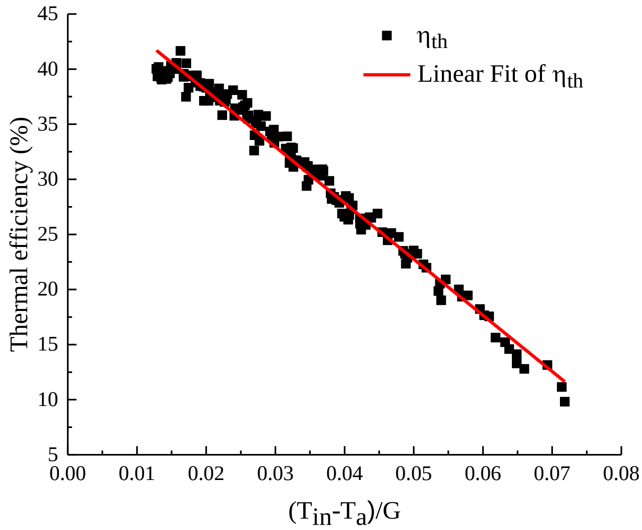

Fig. 12. Plot of instantaneous electrical efficiency of a-Si PV/T collector on April 2

The variations of electrical gain and electrical efficiency are presented in the Fig. 13. There was a significant correlation between electrical gain and solar irradiation. The electrical gain ranged from 30.6W to 77.8W with a daily total electrical gain of 1.55MJ. The electrical efficiency was between 4.62% and 5.92%, and the daily average electrical efficiency according to Eq.(23) was 5.58%.

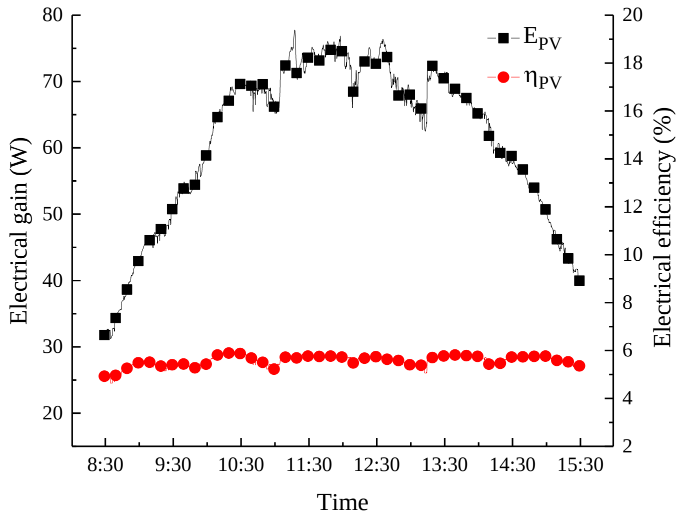

Fig. 13. Variations of electrical gain and electrical efficiency on April 2

In order to clarify the relationship between PV efficiency and the operating temperature, the variations of electrical efficiency and aluminum temperature are compared in Fig. 14. The average temperature of aluminum plate climbed in most of the time, and the maximum could reach 62 °C. While the daily electrical efficiency didn't seem to be influenced by the increment in the operating temperature. The reason may be that the PV/T modules had not been fully exposed to sunlight and were at early-stage degradation. According to predecessors' work, it might take hundreds of hours of exposure for the a-Si cells to reach DSS [20, 25]. In the test, the power generation was expected to be linked with both S-W and thermal annealing effects.

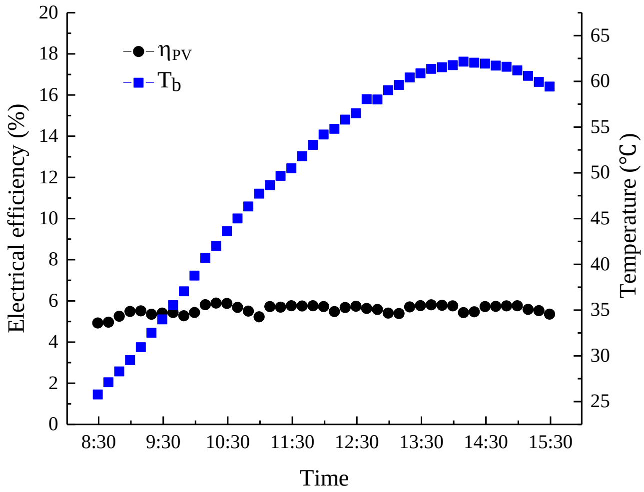

Fig. 14. Variations of electrical efficiency and aluminum plate temperature on April 2

Fig. 15 depicts the I-V characteristic curve of two a-Si PV/T collectors in series. It was measured under the solar irradiation of 880 W/m^2 and the aluminum plate temperature of 47.0 °C at 11:00. The short circuit current, the open circuit voltage and the maximum power were 4.21A, 28.8V and 66.7W, respectively. The experimental results showed that the FF of the a-Si cells was 56%, which is lower than the FF of 61.25% in standard test condition. There could be several factors for this reduction. The operating temperature of the cells was higher than 25 °C. FF generally fell down as the temperature went up due to the change in open circuit voltage and short circuit current [45]. Meanwhile, the cells had been exposed to sunlight before April 2. Some preliminary tests had been conducted in the end of March to ensure that the system can operate properly. Degradation in the cell performance should have taken place, causing a lower FF.

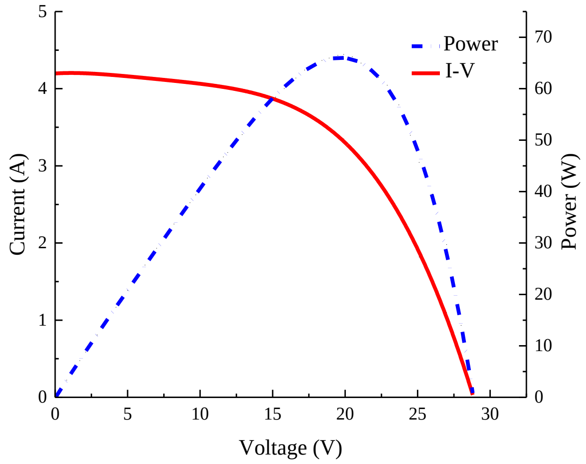

Fig. 15. I-V characteristic curve of the a-Si PV/T collectors on April 2

G=880W/m2 FF=56% V_{oc}=28.8V I_{sc} =4.21A V_{mp}=19.9V I_{mp} =3.35A

5.2 Test on October 27, 2017

After more than half a year operation, a daily performance of the a-Si PV/T system from 8:00 to 15:00 on October 27, 2017 was summarized and investigated in this section. The mass flow rate was the same as that on April 2. Fig. 16 shows the variation of solar irradiation and ambient temperature during the day. The irradiation intensity ranged from 264.6 W/m^2 to 899.0 W/m^2. The daily total solar irradiation was 16.43 MJ/m^2. The ambient temperature fluctuated from 17.5 ^{o}C to 26.6 ^{o}C and the daily average ambient temperature was 23.2 ^{o}C. Fig. 17 and Fig. 18 present simulated and tested temperatures of the aluminum plate, water in the storage tank and at the inlet and outlet of the PV/T system. The final temperatures of water in tank were 54.0 ^{o}C and 54.6 ^{o}C in experiment and simulation, respectively. The maximum temperature of aluminum plate was about 58.0 and 57.7 ^{o}C.

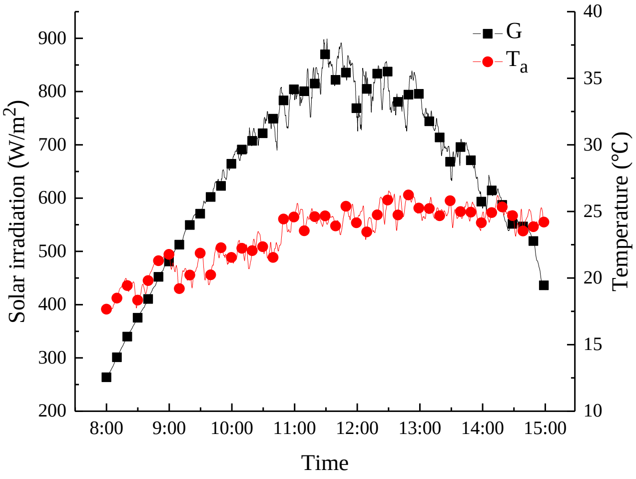

Fig. 16. Variations of solar irradiation intensity and ambient temperature on October 27

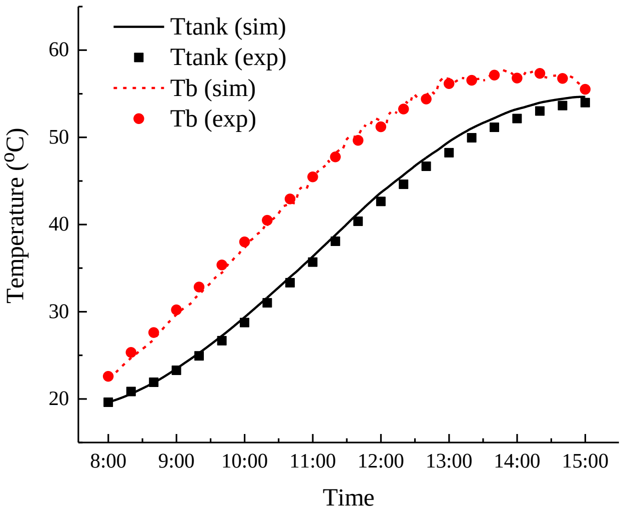

Fig. 17. Simulation and experiment results of the temperatures of the aluminum plate and water in the tank on October 27

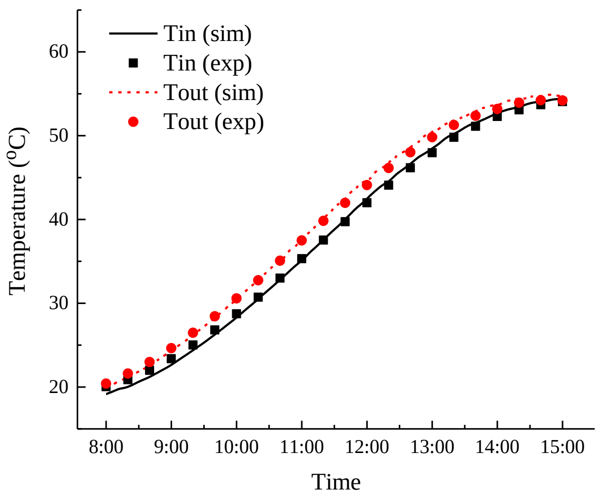

Fig.18. Simulation and experiment results of water temperatures at the inlet and outlet of the PV/T system on October 27

Fig. 19 shows the variation of heat gain and thermal efficiency in the experiment. The maximum heat gain and thermal efficiency were 618.6W and 43.47%. The daily total heat gain of water-storage tank and the daily average thermal efficiency of the a-Si PV/T system were 11.46MJ and 38.65%, respectively. Compared to the results in April 2, the PV/T system had a higher daily thermal efficiency on October 27. This phenomenon can be explained as follows. In both days water temperature in the tank stagnated eventually, when the balance between heat input from solar energy and that lost in the ambient was reached. It means in the end of the test, thermal efficiency of PV/T declined to 0, although solar irradiation may still exceed 450 W/m^2. The final water temperature in the tank over one-day operation was close, which was about 56 ^{o}C and 54 ^{o}C. The daily heat gain in the two days was similar, with a difference of about 0.5 MJ. Nevertheless, the total solar irradiation on April 2 was much stronger. For instance, the duration of solar irradiation above 800 W/m^2 on April 2 was about 4.5 hours (10:00 to 14:30), while it was only 2 hours (11:00-13:00) on October 27. According to Eq.(22), the ratio of the heat gain to the available solar irradiation was higher on October 27. The other reason is that there was more heat loss from the collectors and the connecting tubes to the ambient. As shown in Figs.11 and 19, the instantaneous thermal efficiencies on April 2 and October 27 were close. The average ambient temperature was 19.4 ^{o}C and 23.2 ^{o}C on April 2 and October 27. A lower ambient temperature increased the heat dissipation.

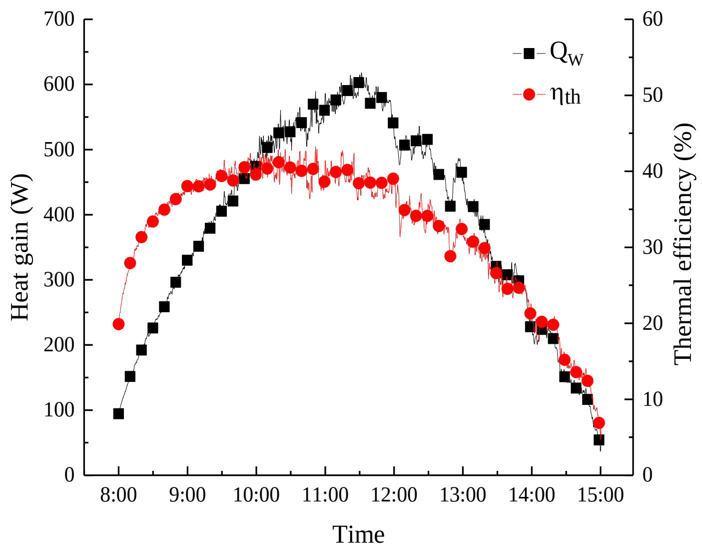

Fig. 19. Variations of heat gain and thermal efficiency on October 27

The thermal efficiency η_{th} against $(T_{in} - T_a)/G$ is shown in the Fig. 20, and it can be determined by Eq.(28). The interception efficiency was close to that in Eq.(27), suggesting that optical efficiencies of PV/T on both days were similar. The coefficient of heat loss was 5.946 W/(m^2·°C). It was higher than that in Eq.(27). For accurate regression, thermal efficiency of the collector should be an approximate quadratic function of $(T_{in} - T_a)/G$, rather than a linear function as denoted by Eq.(27) or Eq.(28). The efficiency curve should have a parabola shape since it dropped more dramatically at higher operating temperature. The slope of the linear fit of thermal efficiency would be steeper when data points at higher (T_{in}- T_a)/G were included, resulting in larger first coefficient of heat loss.

$$\eta_{th} = 0.4793 - 5.946 \frac{T_{in} - T_a}{G} \tag{28}$$

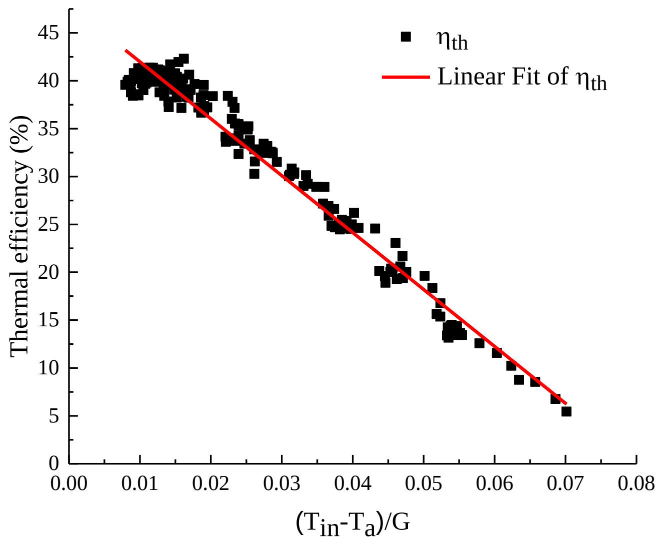

Fig. 20. Plot of instantaneous electrical efficiency of the a-Si PV/T collector on October 27

The variations of electrical gain and electrical efficiency are presented in the Fig. 21. The instantaneous electrical gain ranged from 15.85W to 66.73W with the daily total electrical gain of 1.18MJ. The electrical efficiency was between 4.35% and 5.69%. The lower efficiency generally appeared when the solar irradiation was relatively weak. The daily average electrical efficiency was 5.22%, which was slightly below that on April 2. Differing from the electrical efficiency in Fig.13, there was a more appreciable decrement in efficiency with time in Fig.21. Over half a year outdoor exposure, the cells were supposed to reach the DSS. The operating temperature should play a dominant role in the power generation. Therefore as the water temperature increased, the electricity efficiency was reduced. During 10:00 to 13:20 the irradiation stayed above 650 W/m^2, the water temperature was elevated from about 25 to 50 ^{o}C and the electricity efficiency changed from about 5.5% to 5.2%. The power temperature coefficient of the PV/T was thus estimated to be about -0.22%/ ^{o}C in the daily, short-time scale test.

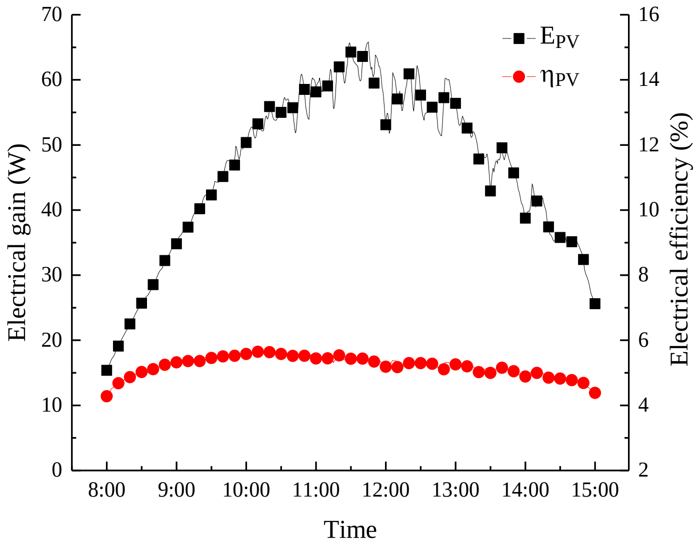

Fig.21. Variations of electrical gain and electrical efficiency on October 27

The I-V characteristic of a-Si PV/T collectors at 11:30 is shown in the Fig. 22. The solar irradiation intensity, FF, open circuit voltage, short circuit current, maximum power point voltage and current are also provided. The aluminum plate temperature was 38 ^{o}C at the moment. The FF of about 57% was slightly higher than that on April 2. The main cause was the lower aluminum plate temperature. Another cause could be the spectrum. Spectral irradiance effects were significant on the seasonal performance of PV cells, especially on a-Si cells [45, 46]. Solar irradiation and short circuit current were lower on October 27.

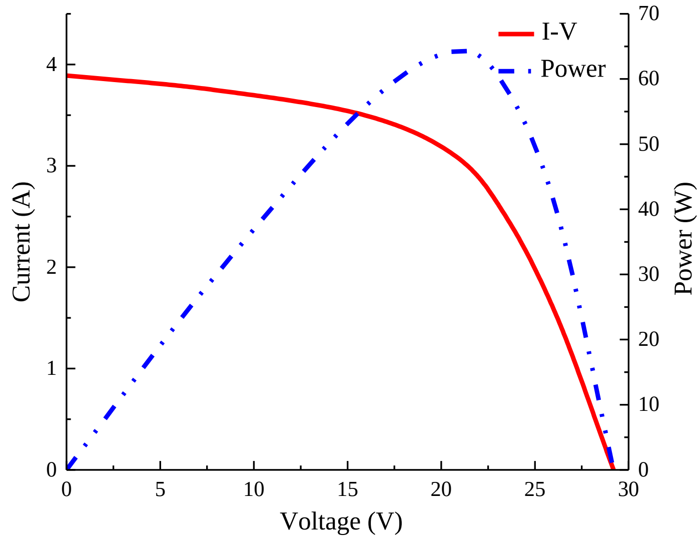

Fig. 22. I-V characteristic curve of the a-Si PV/T collectors on October 27

G=870W/m2 FF=57% V_{oc}=29.2V I_{sc} =3.89A V_{mp}=20.73V I_{mp} =3.1A

As summarized in Table 3, the daily simulation and experiment results of a-Si PV/T system on April 2 and October 27 are compared. The relative deviations of the experimental data from the simulated values are generally less than 2.11%. The daily average electrical efficiency of the simulation is slightly higher than the experiment. The reason may be that the frame shadow is not considered in the simulation. After a half year of operation, there was minor performance degradation of the a-Si cells. No technical problems had occurred during the operating period.

Table 3 Comparison of daily simulation and experiment results of the a-Si PV/T system

Date	4.2			10.27		
	Experiment	Simulation	RE	Experiment	Simulation	RE
$\overline{T_a}$(°C)	19.4			23.2		
H(MJ/m^2)	20.33			16.43		
$T_{w,i}$(°C)	20.2			19.9		
$T_{w,f}$(°C)	56.0	56.5		54.0	54.6	
$\eta_{th,a}$(%)	32.80	33.28	-1.48%	38.65	39.37%	-1.86%
$\eta_{PV,a}$(%)	5.58	5.66	-1.51%	5.22%	5.33%	-2.11%
$\eta_{PVT,a}$(%)	43.87	44.51	-1.46%	49.01	49.94%	-1.90%

5.3 Uncertainty Analysis

The operating temperature, solar irradiation, water flow rate and PV/T module output could be measured directly by the thermocouple, thermal resistance, radiator, flowmeter and power sensor. Their accuracies are shown in Table 2.

The instantaneous heat gain is related to the water temperature increment through the collectors and the mass flow rate. The accuracies of thermal resistance (Pt 100) and flowmeter are ±0.1 °C and ±5%. With minimum increment of about 1 °C, the relative error in the instantaneous heat gain is ±15%.

The total heat gain by the storage tank is associated with the temperature increment over the day. The ultimate increment is around 35 °C on both April 2 and October 27. Given an accuracy of T-type thermocouple of ±0.5 °C, the relative error in the total heat gain is ±1.4%.

The instantaneous and daily average thermal efficiencies are determined by Eqs.(19) and (22) respectively. The derivatives of the efficiencies with respect to the irradiation, temperature increment and flowrate could be deduced accordingly. Therefore, given radiator accuracy of ±2%, the relative error in the instantaneous and daily average thermal efficiencies are ±17% and ±3.4%, respectively. In view of its high accuracy, the daily average thermal efficiency is a better criterion for the thermal performance estimation.

The instantaneous electrical efficiency is expressed by Eq.(21). The relative error is about ±2.1% on the condition of current sensor and radiator accuracies of ±0.1% and ±2%. The daily average electrical efficiency is calculated on the basis of integral of the instantaneous efficiency with time, so the error should be similar.

The fill factor (FF) is determined by Eq.(25). With voltage and current accuracies of ±0.5% and ±2.0%, the relative error in FF is ±5%.

For the sake of good encapsulation of the module, the temperature of the cells was not measured. Instead, the thermocouple was placed at the back of aluminum plate. An evaluation on the temperature difference between the cell and the plate (ΔT) could be carried out. the EVA and black TPT were both 0.2mm thick and their thermal conductivities were 0.23 and 0.36 W/(m·K). Given a heat flux up to 450 W/m^2, ΔT should be less than 1 ^{o}C.

Table 4 Daily experimental results of a-Si PV/T system on some other days

Date	$\overline{T_a}$ (^{o}C)	H(MJ/m^2)	$T_{w,i}$ (^{o}C)	$T_{w,f}$ (^{o}C)	$\eta_{th,a}$(%)	$\eta_{PV,a}$ (%)	$\eta_{PVT,a}$ (%)
4.1	15.7	16.12	21.7	48.8	31.31	5.58	42.37
4.14	23.7	19.56	23.2	55.7	30.95	5.51	41.87
10.22	22.1	16.41	20.4	51.2	34.92	5.25	45.34
10.24	20.7	18.29	20.9	53.3	33.12	5.21	43.46

As mentioned previously, the test results represent the performance of the PV/T system at the early stage of degradation and DSS. Nevertheless, the performance may vary from day to day, as shown in Table 4. Due to the different operation conditions, the daily electrical efficiency and thermal efficiency on other days were not the same as that on April 2 and October 27.

5.4. Further discussion

Although a-Si cells have potential in the medium-high temperature PV/T application, some challenges should be noted: (1) a-Si cells are not the mainstream solar cells; (2) The PV modules have an efficiency around 8%, while conventional c-Si modules on the market have an efficiency of about 17%. In particular, c-Si cells have experienced a much more significant decrement in cost than a-Si cells during the past decade. (3) Knowledge on the practical a-Si PV/T system is lacked. The Staebler-Wronski (S-W) effect on the a-Si PV/T system in the long-term operation still needs to be evaluated.

6. Conclusions

A novel PV/T system using a-Si deposited on stainless steel is introduced in this paper. Tests on the outdoor performance of the system have been carried out and the experimental results for two sunny days (April 2, 2017 and October 27, 2017) are summarized as follows:

1. The peak instantaneous and daily average electricity efficiencies were 5.92% and 5.58% on April 2, and they were 5.69% on 5.22 % on October 27. After more than half a year operation, the daily average electricity efficiency had a 0.36% reduction owing to the S-W effect. The instantaneous electrical efficiency varied slightly with the operating temperature, especially at the early stage of degradation due to the trade-off between the S-W and thermal annealing effects. The power temperature of the PV/T modules after extended exposure was about -0.22%/ ^{o}C on the conditions of solar irradiation of 650W/m^2 and operating temperature from 25 to 50 ^{o}C.

2. The instantaneous thermal efficiency of the PV/T was subject to solar irradiation and operating temperature. In both tests, the water temperature would eventually stagnate around 55 ^{o}C even though the irradiation remained available (>450W/m^2), owing to the balance between the collectors and environment. The maximum instantaneous thermal efficiencies on April 2 and October 27 were close and around 43%. However, the daily average thermal efficiency on April 2 was about 6% lower than that on October 27, attributed to more heat loss from the collectors and pipes.
3. In the more than half a year operation, the electrical and thermal performances of the PV/T have not shown significant degradation. And there was no sign of technical failure. The feasibility of the a-Si PV/T is preliminarily demonstrated by the prototype.
4. The test and simulation are in good agreement. The maximum relative deviation between the experimental and simulated daily thermal efficiency is 1.86%. It is 2.11% in the case of daily electrical efficiency.

7. Acknowledgement

This study was sponsored by EU Marie Curie International Incoming Fellowships Program (703746), National Key R&D Plan (2016YFE0124800), the National Science Foundation of China (51476159, 5171101721, 51776193), and Bureau of International Cooperation, Chinese Academy of Sciences (211134KYSB20160005).

8. References

[1] D.L. King, J.A. Kratochvil, W.E. Boyson. Temperature coefficients for PV modules and arrays: measurement methods, difficulties, and results. in: Proceedings of 25th IEEE Photovoltaic Specialists Conference 1997:1183-1186.

[2] Alibakhsh Kasaeian, Giti Nouri, Parisa Ranjbaran, Dongsheng Wen. Solar collectors and photovoltaics as combined heat and power systems: A critical review. Energy Convers Manage 2018;156:688-705.

[3] Chao Guo, Jie Ji, Wei Sun, Jinwei Ma, Wei He, Yanqiu Wang. Numerical simulation and experimental validation of tri-functional photovoltaic/thermal solar collector. Energy 2015; 87:470-480.

[4] W.C. O'Mara, R.B. Herring, I.P. Hunt. Handbook of semiconductor silicon technology. Park Ridge, New Jersey: Noyes Publications.1990. ISBN 0-8155-1237-6.

[5] Pei Gang, Fu Huide, Zhu Huijuan, Ji Jie. Performance study and parametric analysis of a novel heat pipe PV/T system. Energy 2012; 37:384-395.

[6] Jie Ji, Gang Pei, Wei He, Wei Sun, Guiqiang Li, Jing Li. Research progress on solar photovoltaic/thermal systems utilization. Science Press, Beijing; 2017.08. ISBN: 9787030539793.

[7] Vikrant Sharma, O.S. Sastry, Arun Kumar, Birinchi Bora, S.S. Chandel. Degradation analysis of a-Si, (HIT) hetro-junction intrinsic thin layer silicon and m-C-Si solar photovoltaic technologies under outdoor conditions. Energy 2014; 72:536-546.

[8] S Kichou, S Silvestre, G Nofuentes, M Torres-Ramírez, A Chouder, D Guasch. Characterization of degradation and evaluation of model parameters of amorphous silicon photovoltaic modules under outdoor long term exposure. Energy 2016; 96:231-241.

[9] D.L. Staebler, C.R. Wronski. Reversible conductivity changes in discharge-produced amorphous Si. Appl Phys Lett 1977; 31:292-294.

[10] J.M. Pearce, J. Deng, M.L. Albert, C.R. Wronski, R.W. Collins. Room temperature annealing of fast state from 1 sun illumination in protocrystalline Si:H materials and solar cells. in: Proceedings of 31th IEEE Photovoltaic Specialists Conference 2005:1536-1539.

[11] R. Ruther, G. Tamizh-Mani, J. del Cueto, J. Adelstein, M.M. Dacoregio, B. von Roedern. Performance test of amorphous silicon modules in different climates-year three: higher minimum operating temperatures lead to higher performance levels. in: Proceedings of 31th IEEE Photovoltaic Specialists Conference 2005:1635-1638.

[12] M. Nikolaeva, R.P. Kenny, E. Dunlop, M. Pravettoni. Seasonal variations on energy yield of a-Si, hybrid, and crystalline Si PV modules. Prog Photovolt Res Appl 2010; 18:311-320.

[13] A. Virtuani, L. Fanni. Seasonal power fluctuations of amorphous silicon thin-film solar modules: Distinguishing between different contribution. Prog Photovolt Res Appl 2014; 22:208-217.

[14] B. Kroposki, R. Hansen. Technical evaluation of four amorphous silicon systems at NREL. in: Proceedings of 26th IEEE Photovoltaic Specialists Conference 1997:1357-1360.

[15] J.A. del Cueto, B. von Roedern. Temperature-induced changes in the performance of amorphous silicon multi-junction modules in controlled light-soaking. Prog Photovolt Res Appl 1999; 7:101-112.

[16] B. von Roedern, J.A. del Cueto. Model for Staebler-Wronski degradation deduced from long-term, controlled light-soaking experiments. Mat Res Soc Symp Proc 2000; 609: A10. 4.

[17] G. Makrides, B. Zinsser, A. Phinikarides, M. Schubert, G.E. Georghiou. Temperature and thermal annealing effects on different photovoltaic technologies. Renew Energy 2012; 43:407-417.

[18] Riesen,M. Stuckelberger, F.-J. Haug, C. Ballif, and N. Wyrsch. Temperature dependence of hydrogenated amorphous silicon solar cell performances. J Appl Phys 2016; 119:044505.

[19] R. Platz, D. Fischer, M.A. Zufferey, J.A.A. Selvan, A. Haller. A. Shah. Hybrid collectors using thin-film technology. in: Proceedings of 26th IEEE Photovoltaic Specialists Conference 1997:1293-1296.

[20] M.J.M. Pathak, J.M. Peace, S.J. Harrison. Effect on amorphous silicon photovoltaic performance from high-temperature pulse in photovoltaic thermal hybrid devices. Sol Energy Mater Sol Cells 2012; 100:199-203.

[21] R.P. Kenny, A.L. Chatzipanagi, T. Sample. Preconditioning of thin-film PV module technologies for calibration. Prog Photovolt Res Appl 2014; 22:166-172.

[22] S. Wagner, D.E. Carlson, H.M. Branz. Amorphous and microcrystalline silicon solar cells. in: Electrochemical Society of International Symposium 1999, Seattle, Washington. NREL/CP-250-29589.

[23] D. Ronak, I. Adnan, L.J. Goh, M.H. Ruslan, S. Kamaruzzaman. Predicting the performance of amorphous and crystalline silicon based photovoltaic solar thermal collectors. Energy Convers Manage 2011; 52:1741-1747.

[24] J. Rozario, A.H. Vora, S.K. Debnath, M.J.M. Pathak, J.M. Pearce. The effect of dispatch strategy on electrical performance of amorphous silicon-based solar photovoltaic-thermal systems. Renew Energy 2014; 68:459-465.

[25] M.J.M. Pathak, K. Girotra, S.J. Harrison, J.M. Peace. The effect of hybrid photovoltaic thermal device operating conditions on intrinsic layer thickness optimization of hydrogenated amorphous silicon solar cells. Sol Energy 2012; 86:2673-2677.

[26] C. Frigeri, M. Serenyi, Z. Szekrenyes, K. Kamaras, A, Csik, N.Q. Khanh. Effect of heat treatments on the properties of hydrogenated amorphous silicon for PV and PVT applications. Sol Energy 2015: 119:225-232.

[27] Jianhui Hu, Wujun Chen, Zhenyu Qiu, Bing Zhao, Jinyu Zhou, Yegao Qu. Thermal performances of ETFE cushion roof integrated amorphous silicon photovoltaic. Energy Convers Manage 2015; 106:1201–1211.

[28] Bing Zhao, Wujun Chen, Jianhui Hu, Zhenyu Qiu, Yegao Qu, Binbin Ge. A thermal model for amorphous silicon photovoltaic integrated in ETFE cushion roofs. Energy Convers Manage 2015; 100:440–448.

[29] Morteza Abdolzadeh, Mohsen Sadeqkhani, Alireza Ahmadi. Computational modeling of a BIPV/T ethylene tetrafluoroethylen (ETFE) cushion structure roof. Energy 2017; 133:998-1012.

[30] Wei Liao, Shen Xu. Energy performance comparison among see-through amorphous-

silicon PV (photovoltaic) glazings and traditional glazings under different architectural conditions in China. Energy 2015; 83:267-275.

[31] Ershuai Yin, Qiang Li, Yimin Xuan. Thermal resistance analysis and optimization of photovoltaic thermoelectric hybrid system. Energy Convers Manage 2017; 143:188-202.

[32] Enok J.H. Skjølstrup, Thomas Søndergaard. Design and optimization of spectral beamsplitter for hybrid thermoelectric-photovoltaic concentrated solar energy devices. Sol Energy 2016; 139:149-156.

[33] Debashree Banerjee, Örjan Vallin, Kabir Majid Samani, Subimal Majee, Shi-Li Zhang, Johan Liu, Zhi-Bin Zhang. Elevated thermoelectric figure of merit of n-type amorphous silicon by efficient electrical doping process. Nano Energy 2018; 44:89-94.

[34] Bjørk, R., Nielsen, K.K. The performance of a combined solar photovoltaic (PV) and thermoelectric generator (TEG) system. Sol Energy 2015; 120:187-194.

[35] M Wang, J Peng, N Li, L Lu, H Yang. Experimental study on thermal performance of semi-transparent PV window in winter in Hong Kong. Energy Procedia 2017; 105:864-868.

[36]Yoon, J.-H., Song, J., Lee, S.-J. Practical application of building integrated photovoltaic (BIPV) system using transparent amorphous silicon thin-film PV module. Sol Energy 2011; 85(5):723-733.

[37] W Zhang, B Hao, N Li. Experiment and simulation study on the amorphous silicon photovoltaic walls. Int J Photoenergy 2014; 2014:643637.

[38] T. Nualboonrueng, P. Tuenpusa, Y. Ueda, A. Akisawa. Field experiments of PV-Thermal collectors for residential application in Bangkok. Energies 2012; 5:1229-1244.

[39] X Wu, G Gong，C Wang. Experiment and performance analysis of amorphous silicon solar PV-thermal hybrid system. Taiyangneng Xuebao/Acta Energiae Solaris Sinica 2017; 38(2):363-371.

[40] Xunlight Corporation. www.xunlightchina.com, 2015.2.

[41] Runsheng Tang, Tong Wu. Optimal tilt-angles for solar collectors used in China. Appl Energy 2004; 79: 239-248.

[42] TL Bergman, FP Incropera, DP DeWitt, AS Lavine. Fundamentals of heat and mass transfer. John Wiley & Sons; 2011.

[43] ANSI/ASHRAE 93-2010 Methods of testing to determine the thermal performance of solar collectors. New York: ASHRAE; 2010.

[44] J. Jie, L Jianping, T.T. Chow, H. Wei, P. Gang. A sensitivity study of a hybrid photovoltaic/thermal water-heating system with natural circulation. Appl Energy 2007; 84:222-237.

[45] P. Singh, N.M.Ravindra. Temperature dependence of solar cell performance—an analysis. Sol Energy Mater Sol Cells 2012; 101:36–45.

[46] R. Ekea, T.R. Betts, R. Gottschalg. Spectral irradiance effects on the outdoor performance of photovoltaic modules. Renew Sust Energy Rev 2017; 69:429–434.